








Histological characterization of the human scapholunate ligament

Jesús Chato-Astrain^{1,2}  | Olga Roda³  | Víctor Carriel^{1,2}  |
Fidel Hita-Contreras⁴  | Indalecio Sánchez-Montesinos^{2,3}  |
Miguel Alaminos^{1,2}  | Pedro Hernández-Cortés^{2,5,6} 

¹Tissue Engineering Group, Department of Histology, Faculty of Medicine, University of Granada, Granada, Spain

²Instituto de Investigación Biosanitaria ibs.GRANADA, Granada, Spain

³Department of Human Anatomy and Embryology, Faculty of Medicine, University of Granada, Granada, Spain

⁴Department of Health Sciences, Faculty of Health Sciences, University of Jaén, Jaén, Spain

⁵Department of Surgery and Surgical Specialties, Faculty of Medicine, University of Granada, Granada, Spain

⁶Division of Traumatology and Orthopedic Surgery, San Cecilio University Hospital, Granada, Spain

Correspondence

Indalecio Sánchez-Montesinos, Miguel Alaminos and Pedro Hernández-Cortés, University of Granada and Instituto de Investigación Biosanitaria ibs.GRANADA, Granada E18016, Spain.
Email: ismg@ugr.es, malaminos@ugr.es and phc@ugr.es

Funding information

CTS-115, Tissue Engineering Group of the University of Granada, Spain. Funding for open access charge: Universidad de Granada / CBUA.

Review Editor: Paolo Bianchini

Abstract

The scapholunate interosseous ligament (SLIL) plays a fundamental role in stabilizing the wrist bones, and its disruption is a frequent cause of wrist arthrosis and dysfunction. Traditionally, this structure is considered to be a variety of fibrocartilaginous tissue and consists of three regions: dorsal, membranous and palmar. Despite its functional relevance, the exact composition of the human SLIL is not well understood. In the present work, we have analyzed the human SLIL and control tissues from the human hand using an array of histological, histochemical and immunohistochemical methods to characterize each region of this structure. Results reveal that the SLIL is heterogeneous, and each region can be subdivided in two zones that are histologically different to the other zones. Analysis of collagen and elastic fibers, and several proteoglycans, glycoproteins and glycosaminoglycans confirmed that the different regions can be subdivided in two zones that have their own structure and composition. In general, all parts of the SLIL resemble the histological structure of the control articular cartilage, especially the first part of the membranous region (zone M1). Cells showing a chondrocyte-like phenotype as determined by S100 were more abundant in M1, whereas the zone containing more CD73-positive stem cells was D2. These results confirm the heterogeneity of the human SLIL and could contribute to explain why certain zones of this structure are more prone to structural damage and why other zones have specific regeneration potential.

Research Highlights

Application of an array of histological analysis methods allowed us to demonstrate that the human scapholunate ligament is heterogeneous and consists of at least six different regions sharing similarities with the human cartilage, ligament and other anatomical structures.

KEYWORDS

histochemistry, immunohistochemistry, scapholunate ligament

Jesús Chato-Astrain and Olga Roda contributed equally to this study.

This is an open access article under the terms of the [Creative Commons Attribution](https://creativecommons.org/licenses/by/4.0/) License, which permits use, distribution and reproduction in any medium, provided the original work is properly cited.

© 2023 The Authors. *Microscopy Research and Technique* published by Wiley Periodicals LLC.

1 | INTRODUCTION

The physiological function of the human wrist is strictly dependent on the complex anatomy of the carpal bones and the ligaments providing stability to these bones (Andersson, 2017). The human scapholunate interosseous ligament (SLIL) is a C-shape structure connecting the scaphoid and lunate carpal bones, and it is considered as the primary stabilizer of the scapholunate joint (Johnson et al., 2013). SLIL disruption due to trauma or degeneration is considered the most common cause of carpal instability, which can significantly compromise hand function and lead to wrist arthrosis (Kitay & Wolfe, 2012; Wolff & Wolfe, 2016). The regenerative capability of the human SLIL is very limited, and injuries in this structure cannot heal by themselves and typically require surgical treatment (Mullikin et al., 2020). Although, numerous surgical procedures have been described (Lui et al., 2019; Mullikin et al., 2020), reconstruction of the dorsal component of the SLIL is the usual surgical treatment for SLIL injuries, underestimating the biomechanical role of the membranous and palmar portions of this structure (Naqui et al., 2018).

Despite its key role in carpal physiology, the exact structure and composition of the human SLIL are not fully understood. The gross morphology of the SLIL was originally defined by Berger and cols. (Berger, 1996), who described three major zones in the human SLIL: the dorsal, membranous, and palmar regions. The dorsal region is transversely oriented, whereas the palmar region is oblique, allowing significant relative movement between the two bones (Sokolow & Saffar, 2001). Numerous reports focused on the study of the SLIL from the anatomical, kinematical and biomechanical standpoints (Kitay & Wolfe, 2012; Rajan & Day, 2015; Wolff & Wolfe, 2016).

Histologically, the human SLIL is thought to be composed of collagen fascicles infiltrated by loosely organized connective tissue, as it is the case of most other intraarticular ligaments, although the SLIL could also share some similarities with human fibrocartilage (Berger, 1996; Sokolow & Saffar, 2001). However, the detailed histological structure of the human SLIL remains to be elucidated.

In the present work, we carried out a comprehensive histological characterization of the human SLIL using an array of histochemical and immunohistochemical methods in order to determine the main extracellular matrix molecules and cells which form part of this ligament.

2 | MATERIALS AND METHODS

2.1 | Tissue samples and histological analysis

We used six hand specimens obtained from six fresh-frozen cadavers, who provided informed consent to use their organs and tissues for scientific purposes (McHanwell et al., 2008; Riederer et al., 2012). The specimens had no previously documented hand injuries or surgeries. All specimens were thawed at room temperature and dissected in the Human Anatomy Department of the School of Medicine of the University of Granada (Spain). Specifically, the carpal bones were dissected, and the scaphoid and lunate bones joined by the SLIL were

carefully extracted and transferred to the Laboratory of Histology of the Medical School of the University of Granada. Then, the SLIL were carefully separated from the carpal bones and fixed in 10% buffered formalin (Panreac Química S.L.U., Barcelona, Spain) for histological analysis. As controls, several structures were also dissected and extracted from the same human hands, including samples of the flexor tendon (FT), carpal ligament (CL), articular cartilage (AC), triangular fibrocartilage (TF), carpal articular capsule (CC) and retinaculum (RT). These tissues were fixed and processed using the same protocols used for the SLIL. Authorization was obtained from the Department of Anatomy of the Medical School of the University of Granada, which approved the study.

Formalin-fixed SLIL and control tissues were dehydrated, cleared in xylene and embedded in paraffin following routine histological methods. 5 μ m-thick sections were obtained from each sample, dewaxed in ethanol series, rehydrated, and stained with hematoxylin and eosin (HE) (Panreac Química S.L.U.) using standard protocols. In brief, samples were dewaxed, rehydrated, and stained with hematoxylin for 3 min. Samples were then differentiated in tap water for 5 min and stained with eosin for 1 min. Finally, slides were dehydrated and coverslipped. Histological images were then obtained using a Panoramic Desk DW II histological scanner (3DHISTECH, Budapest, Hungary) from controls and from the human SLIL, and images were taken from the 6 main zones of the SLIL (Figure 1): dorsal region -part 1- (D1), dorsal region -part 2- (D2), membranous region -part 1- (M1), membranous region -part 2- (M2), palmar region -part 1- (P1) and palmar region -part 2- (P2).

2.2 | Histochemistry

To evaluate the presence and distribution of relevant components of the extracellular matrix (ECM), all tissue samples were subjected to histochemical methods. To identify the tissue elastic fibers, samples were stained using Verhoeff histochemical staining method (VHF). To reveal the presence of fibrillar collagens, we used picosirius red (PSR). Non-fibrillar ECM components were evaluated using several histochemical methods. To identify ECM proteoglycans, we used alcian blue staining (AB) at pH 2.5, whereas the periodic acid-Schiff staining (PAS) was used to stain glycoproteins. In addition, Safranin O staining (SO) was used to identify cartilage components. All these methods were performed following previously published standard histochemical methods (Blanco-Elices et al., 2022; Carriel et al., 2011; García-García et al., 2021; Sánchez-Porras et al., 2023). In brief, VHF was performed by incubating deparaffinized tissues in Verhoeff staining solution for 10 min and further differentiation in 2% ferric chloride for 15 sec. PSR was carried out by incubating the samples in sirius red F3B for 30 min and counterstaining with Harris's hematoxylin for 5 min. For the AB analysis, samples were incubated in alcian blue working solution for 30 min and counterstained with nuclear fast red for 1 min. For SO, histological sections were first stained with Weigert iron hematoxylin staining solution for 10 min, contrasted with light green solution for 5 min, and stained with 0.1% safranin O solution

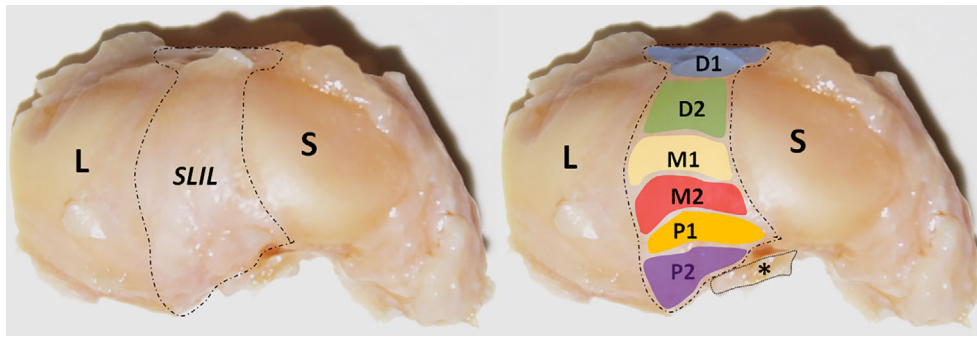


FIGURE 1 Macroscopic images of the human scapholunate interosseous ligament (SLIL) analyzed in this work. The left image shows the lunate bone (L) attached to the scaphoid bone (S) by the SLIL. The image to the right shows the different zones within each region of the SLIL. The asterisk corresponds to the radio-scapho-lunate ligament. D1, dorsal region (part 1); D2, dorsal region (part 2); M1, membranous region (part 1); M2, membranous region (part 2); P1, palmar region (part 1); P2, palmar region (part 2).

for 10 min after a rinse in 1% acetic acid solution. PAS was performed by incubating each tissue in 0.5% periodic acid solution for 5 min, followed by incubation in Schiff reagent for 15 min and counterstaining with Harris hematoxylin for 1 min.

2.3 | Immunohistochemistry

Indirect immunohistochemistry was performed for the specific identification of ECM components and cell phenotype. In relation to the ECM fibers, collagen types I, II III and IV were identified using this method. In addition, immunohistochemistry was used to identify two specific proteoglycans, including versican (VCAN) and aggrecan (ACAN), two glycosaminoglycans playing an important role in cartilage, including keratan-sulphate (KS) and chondroitin-6-sulphate (C6S). The ECM glycoprotein tenascin-C was also identified using immunohistochemistry. To identify specific cell phenotypes, immunohistochemical methods were used for the proteins CD73 (marker of stemness and undifferentiation), S100 (marker of chondrogenic and neural crest lineage) and CD34 a well-known marker of blood vessels (García-Martínez et al., 2017; Vela-Romera et al., 2019). All immunohistochemical analyses were carried out using routine methods and were conducted using the same conditions for all samples. Briefly, tissue sections were dewaxed and rehydrated, and antigen retrieval was performed as detailed in Supplementary Table S1. Endogenous peroxidases were quenched with H_2O_2 (Panreac Química S.L.U.) and prehybridization was performed with a solution containing casein and horse serum (Vector laboratories, Burlingame, CA, USA). Samples were then incubated overnight with a specific primary antibody (Supplementary Table S1). After washing, sections were then incubated with ready-to-use anti-rabbit and anti-mouse secondary antibodies labeled with peroxidase (Vector Laboratories), and a diaminobenzidine (DAB) substrate kit (Vector Laboratories) was used to reveal the immune reaction. Finally, samples were briefly counterstained with Harris hematoxylin (Thermo Fisher Scientific, Waltham, MA) for 15 s, followed by 3 min in tap water, and coverslipped. An example of the blanks used for the quantification of each immunostaining was included in Supplementary Figure S1.

2.4 | Quantitative analyses

Results of the histochemical analyses were quantified in each zone of the SLIL and control tissues using the ImageJ software (version 1.53 k, National Institute of Health, Bethesda, MD), as previously described (V. Carriel et al., 2014; Ortiz-Arrabal et al., 2021; Rodríguez-Pozo et al., 2020; Ruiz-López et al., 2022). In each image, we randomly selected five $25 \mu m \times 25 \mu m$ square areas, and we obtained a numeric value (expressed as intensity units or I.U.) corresponding to the average pixel intensity within each square using the square tool of the software. Results were then subtracted from the blank values and averages and standard deviations were calculated for each group of samples. A total of 30 measurements were obtained for each type of tissue (controls and SLIL zones). Results corresponding to the analysis of cell phenotypes as determined by CD73 and S100 immunohistochemistry were quantified by determining the percentage of positive cells found at in each region of the SLIL. In short, we counted the total number of cells showing positive signal within a $300 \mu m \times 300 \mu m$ area randomly selected on each region, then the number of positive cells was calculated per unit of area. The same method was used to quantify the number of blood vessels found at each SLIL region in samples subjected to CD34 immunohistochemistry.

2.5 | Hierarchical clustering

In order to identify differences and similarities among the different samples analyzed here (SLIL zones and controls) based on their global histochemical and immunohistochemical profiles, we analyzed all samples using hierarchical clustering. With this purpose, average results obtained for each quantitative histochemical and immunohistochemical analyses showing statistically significant differences among the samples were analyzed using ClustVis web tool for clustering of multivariate data (Metsalu & Vilo, 2015) (Accessible at <https://biit.cs.ut.ee/clustvis/>). A Heatmap dendrogram displaying relative quantification for each marker was generated by the software based on hierarchical clustering analysis using the Euclidean distance and the complete clustering method for both the rows and columns.

2.6 | Statistical analysis

Results obtained for each SLIL region subjected to each analytical technique were statistically compared with each control tissue. The two regions that we analyzed from each of the zones originally established by Berger were also compared (D1 vs. D2, M1 vs. M2 and P1 vs. P2). First, we evaluated the normality of each distribution using the Shapiro–Wilk test. As none of the distributions fulfilled the criteria of normality, comparison between two specific groups of samples were carried out using the non-parametric test of Mann–Whitney. The comparisons were done with Real Statistics Resource Pack software (Release 7.2) (Dr. Charles Zaiontz, Purdue University, West Lafayette, IN, USA), available at www.real-statistics.com. A Bonferroni-adjusted statistical significance p value below .001 was set for all double-tailed tests, since multiple comparisons were carried out at the same time.

3 | RESULTS

3.1 | Histological structure of the human SLIL

Analysis of the human SLIL using HE staining confirmed that this structure was histologically heterogeneous, with several histological differences found among the zones analyzed in this work (Figure 2). When the dorsal region of the SLIL was analyzed, we first found that the D1 zone consisted of a dense ECM with abundant fibers oriented in different spatial directions and a scarce population of elongated or

spindle-shaped cells dispersed across the ECM (Figure 2a,g). Then, D2 showed an ECM containing abundant well aligned and oriented fibers (Figure 2b,h), and an abundant population of spindle-shaped cells displaying similarities with the cells in D1. At the membranous region, we found that M1 contained a dense ECM with no identifiable fibers and rounded cells scattered within the tissue ECM (Figure 2c,i). Interestingly, these cells tended to form groups resembling the human hyaline cartilage isogenic groups, with clusters of 2–4 cells surrounded by a clear ECM with a peripheral capsule that was very similar to the structure found in normal human cartilage. In turn, the M2 zone showed a very dense ECM with fibers apparently oriented in layers with different spatial directions (Figure 2d,j). Cells found in M2 were not abundant and tended to form rows that partially resembled human fibrochondrocytes and were also surrounded by a pericellular capsule (Figure 2d,j). Finally, the palmar region of the SLIL contained abundant fibers and scattered spindle-shaped cells. For P1, we found abundant cells within a dense ECM with properly oriented fibers (Figure 2e,k). However, analysis of the P2 zone revealed the presence of fewer elongated or rounded cells, and the fibers were oriented to different spatial directions (Figure 2f,l).

3.2 | Analysis of the human scapholunate ligament ECM

First, our analysis of elastic fibers as determined by VHF histochemistry showed very low amount of these ECM components in all samples,

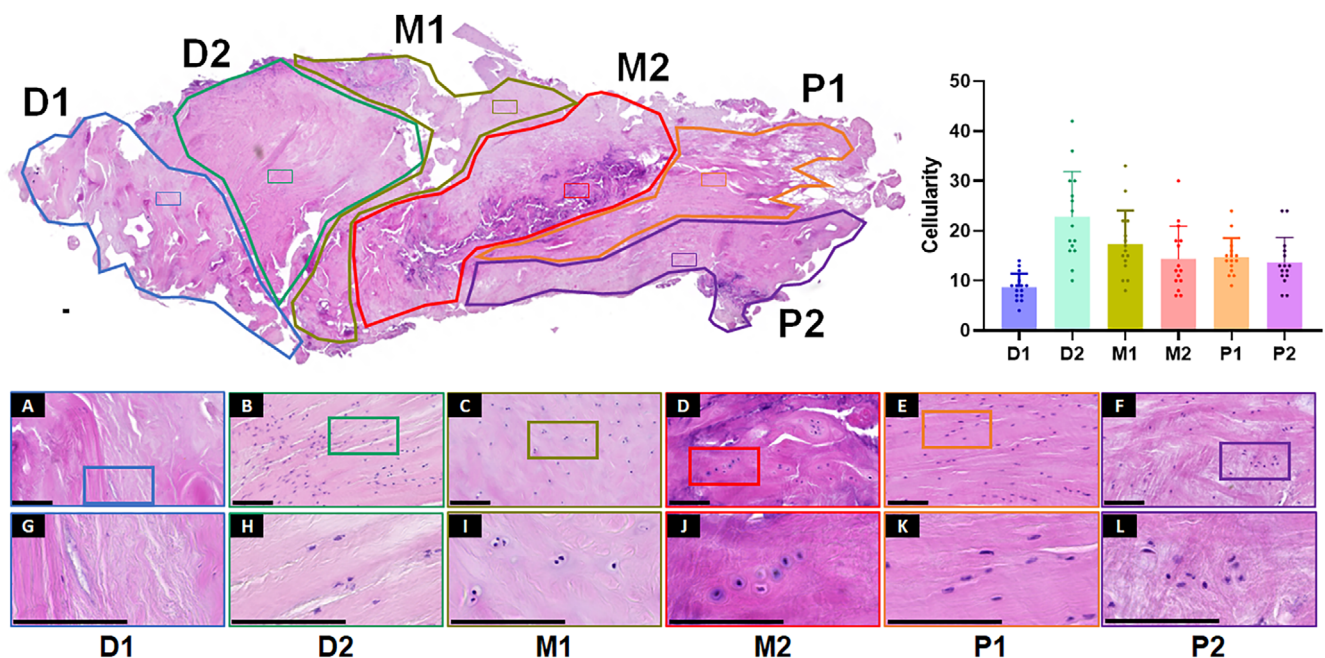


FIGURE 2 Histological analysis of the human scapholunate ligament (SLIL) stained with hematoxylin–eosin staining showing the 6 zones analyzed in the present work. Illustrative high-augmentation images are also shown for each zone. D1, dorsal region (part 1) (a and g); D2, dorsal region (part 2) (b and h); M1, membranous region (part 1) (c and i); M2, membranous region (part 2) (d and j); P1, palmar region (part 1) (e and k); P2, palmar region (part 2) (f and l). Scale bars: 100 μ m. The histogram to the right corresponds to the quantification of the number of cells per unit of area in each zone of the SLIL.

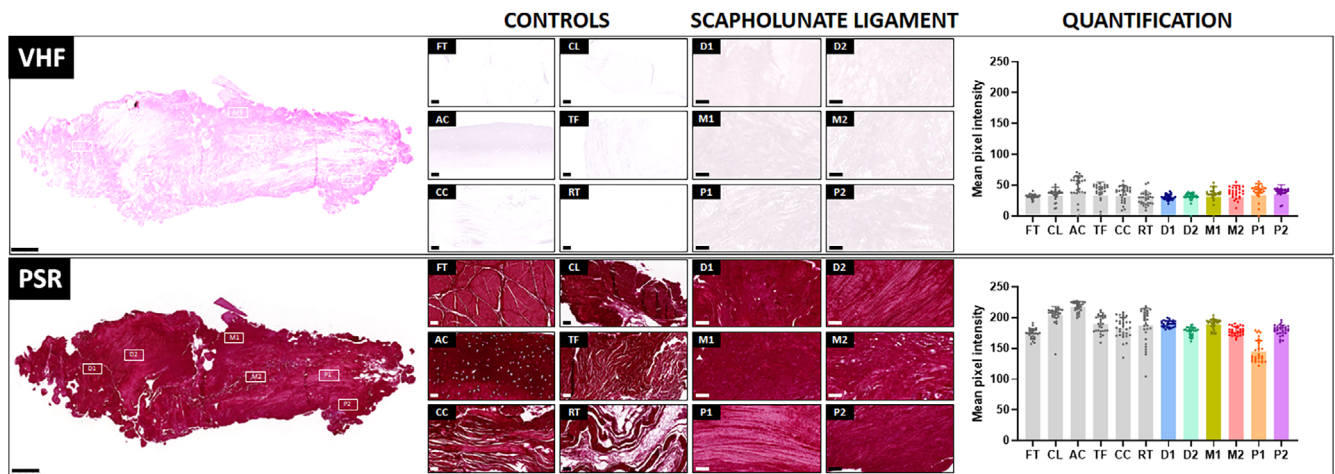


FIGURE 3 Analysis of elastic and collagen fibers in the human scapholunate ligament (SLIL) and control tissues using Verhoeff (VHF) and picrosirius red (PSR) histochemistry, respectively. Histograms represent the results of the staining signal quantification for each analysis method. AC, articular cartilage; CC, carpal articular capsule; CL, carpal ligament; FT, flexor tendon; D1, dorsal region (part 1); D2, dorsal region (part 2); M1, membranous region (part 1); M2, membranous region (part 2); P1, palmar region (part 1); P2, palmar region (part 2); RT, retinaculum; TF, triangular fibrocartilage. Scale bars: 1000 μm in the SLIL global image and 100 μm in the high magnification images.

with no differences among samples (Figure 3 and Table 1). Elastic fibers were thin and parallelly oriented to the longitudinal axis of the abundant collagen network. In contrast, the quantitative analysis of fibrillar collagen fibers identified by PSR histochemical staining revealed that all control tissues and the six regions of the SLIL analyzed here contained high amounts of collagen (Figure 3). Differences were statistically significant for most zones, especially for P1, which showed significantly lower amounts of collagen than the six control tissues (Table 1). Interestingly, comparisons between the two zones distinguished within each region in this study (D1 vs. D2, M1 vs. M2 and P1 vs. P2) were statistically significant for the amount of fibrillar collagen fibers identified by PSR (Table 1).

Then, we quantified four specific types of collagens by immunohistochemistry, and we found that, in general, the most predominant collagen fiber in SLIL was Col-II (Figure 4 and Table 1). For Col-I, we found that most SLIL regions significantly differed from all control tissues, with regions D2, P1 and P2 showing the lowest amounts of this type of collagen, and AC showed high contents of Col-I. Within the SLIL regions, we found that D1 was significantly higher than D2. Collagen type II was positive in almost every region of the SLIL, with the lowest values found in P1 region. Interestingly, Col-II expression in M1 region was high, as it was the case of the AC control samples, followed by D2 region, with non-significant differences between AC and M1 or D2. Regarding Col-III, most SLIL regions expressed low amounts of these fibrillar components. Among the different SLIL regions, M2 exhibited the most positive expression of this ECM component, although at lower levels than Col-IV. Most control tissues tended to express high amounts of type-III collagen, with the only exception of AC, which was highly positive for collagens types I and II and showed lower amounts of collagens types III and IV. Differences were significant for most comparisons, including the comparisons within each region, but were non-significant for the comparison of AC versus D2, M1 and P1. For Col-IV, we found that most control tissues and SLIL zones contained very few amounts of this protein, whilst M2 was highly positive. Differences between M2 and all

types of control tissues were statistically significant, as well as the differences between M1 and M2 (Table 1).

When the ECM proteoglycans were globally identified by AB histochemistry (Figure 5 and Table 1), we found that most regions of the SLIL were enriched in these non-fibrillar components of the tissue ECM, especially in zones M1, M2 and P2. However, the presence of these components tended to be low in most control tissues, except for AC, which showed significantly higher amounts of proteoglycans than all regions of the SLIL. In addition, M1, M2 and P2 were statistically higher than all control tissues except AC, whereas D2 was higher than D1 and P2 was higher than P1. On the other hand, ECM molecules identified with SO staining showed a very positive reaction for cartilage components and collagen fibers. Interestingly the quantification of the SO positive reaction followed a similar pattern than AB histochemistry, although at higher levels. M1 region exhibited the highest SO intensity, with significant differences with all control tissues (Table 1). Interestingly, the SO staining pattern was similar in M1 and AC, with an intense area stained in red devoid from collagen fibers stained in green (Figure 5). In addition, the analysis of glycoproteins using PAS histochemistry (Figure 5 and Table 1) revealed that the highest expression corresponded again to AC control tissues. For the SLIL zones, M2, P1 and P2 showed the highest glycosaminoglycans content, with statistical differences with all the control tissues. Differences were also statistically significant for the comparison within each SLIL region (P1 vs. P2, M1 vs. M2, and D1 vs. D2).

Then, we specifically detected some of the most important proteoglycans, glycosaminoglycans and glycoproteins in SLIL ECM by indirect immunohistochemistry. First, when versican was analyzed, we found that this protein playing an important role in ECM homeostasis was highly positive in D2 and P1, with significant differences with AC, CL and RT in both cases, whereas very low amounts of VCAN were found in M1, which statistically differed from all control tissues except RT. Comparisons within the SLIL regions revealed statistical differences between M1 and M2 and between P1 and P2 (Figure 6 and Table 1).

TABLE 1 Quantitative analysis of extracellular matrix (ECM) components in the human scapholunate ligament (SLIL) zones and control tissues.

	VHF	PSR	COL-I	COL-II	COL-III	COL-IV	AB	SO	PAS	VCAN	ACAN	KS	C6S	TNC
FT	31.63 ± 3.46	174.29 ± 7.94	83.71 ± 8.29	66.27 ± 40.91	87.45 ± 24.08	12.83 ± 6.87	34.05 ± 5.91	86.77 ± 16.48	56.4 ± 1.72	59.97 ± 33.27	8.47 ± 3.28	91.1 ± 17.29	74.17 ± 12.24	0.97 ± 1.5
CL	33.03 ± 13.53	204.42 ± 13.66	96.09 ± 14.42	81.8 ± 34.85	92.87 ± 15.14	32.97 ± 26.45	38.8 ± 3.22	62.33 ± 26.95	72.19 ± 4.87	56.57 ± 17.64	44.93 ± 20.12	126.9 ± 5.42	114.37 ± 16.15	21.77 ± 3.67
AC	38.23 ± 26.8	217.87 ± 8.02	95.9 ± 27.36	104.5 ± 31.79	48.65 ± 5.39	15.73 ± 3.55	144.46 ± 4.49	235.13 ± 7.51	119.6 ± 6.51	40.17 ± 5.63	83.5 ± 16.4	128.8 ± 9.19	88.17 ± 3.11	9.07 ± 2.66
TF	33.43 ± 21.4	190.05 ± 13.78	69.26 ± 9.06	81.67 ± 37.32	102.32 ± 11.56	4.83 ± 10.86	51.48 ± 9.74	160.57 ± 19.63	76.75 ± 19.63	74.9 ± 27.38	10.23 ± 6.66	115.2 ± 7.9	116.53 ± 11.82	12.97 ± 8.51
CC	32.4 ± 16.72	183.48 ± 17	70.06 ± 11.2	74.83 ± 35.27	99.5 ± 16.87	43 ± 41.4	49.48 ± 6.17	148.2 ± 18.04	71.2 ± 14.16	92.47 ± 23.89	12.27 ± 6.84	111.13 ± 6.12	107.53 ± 6.79	4.03 ± 1.5
RT	28.37 ± 10.2	187.44 ± 27.94	90.28 ± 19.36	51.33 ± 39.25	130.66 ± 23.94	17.87 ± 25.02	30.51 ± 2.51	133.6 ± 26.02	45.74 ± 11.93	36.93 ± 21.69	11.63 ± 9.48	66.9 ± 9.27	79.87 ± 8.32	58.97 ± 30.15
D1	30.4 ± 4.41	189.94 ± 5.08	61.43 ± 8.19	88.6 ± 9.16	56.91 ± 6.56	17.4 ± 22.5	48.77 ± 2.37	173.93 ± 37.27	69.85 ± 7.88	59.57 ± 21.43	87.13 ± 13.44	126.47 ± 6.68	93.57 ± 7.19	24.93 ± 4.33
D2	31.23 ± 7.16	177.89 ± 6.79	48.58 ± 7.32	95.33 ± 11.28	48.97 ± 6.22	24.53 ± 18.77	66.6 ± 22.08	195.87 ± 38.35	80.43 ± 6.82	74.8 ± 20.52	46 ± 20.54	112.53 ± 3.78	92.1 ± 7.26	5.53 ± 1.81
M1	31.37 ± 16.56	189.23 ± 8.14	56.27 ± 16.45	103.7 ± 11.08	46.65 ± 7.03	18.63 ± 14.07	80.94 ± 8.2	249.33 ± 0.71	84.12 ± 7.02	30.03 ± 4.75	119 ± 10.36	112.07 ± 4.07	103.1 ± 4.74	11.13 ± 14.45
M2	30.97 ± 18.63	178.29 ± 6.92	70.09 ± 7.53	71.03 ± 15.42	68.54 ± 10.22	173.9 ± 36.25	88.9 ± 13.99	195.27 ± 43.8	97.4 ± 6.28	54.67 ± 30.59	30.43 ± 8.09	113.93 ± 4.35	104.67 ± 4.6	29.47 ± 11.42
P1	33.67 ± 18.51	145.15 ± 18.13	45.2 ± 5.54	64.57 ± 13	45.9 ± 4.41	46.63 ± 31.87	54.67 ± 6.94	93.53 ± 60.8	101.96 ± 9.86	80.47 ± 20.57	3.87 ± 5.14	108.33 ± 7.54	101.57 ± 4.05	0.33 ± 1.83
P2	35.13 ± 15.57	179.75 ± 8.27	43.82 ± 6.93	81.83 ± 13.04	56.06 ± 6.11	50.8 ± 25.39	111.37 ± 11.02	211.7 ± 14.68	92.72 ± 5.09	51.1 ± 24.87	15.57 ± 5.32	115.9 ± 4.16	103 ± 4.4	0.03 ± 0.18
AC versus D1	.0026	<.0001*	<.0001*	<.0001*	<.0001*	.0076	<.0001*	<.0001*	<.0001*	.0001*	.3429	<.0001*	.0017	<.0001*
CC versus D1	.0551	.1194	<.0001*	<.0001*	<.0001*	<.0001*	.2132	<.001*	.7747	<.0001*	<.0001*	<.001*	<.0001*	<.0001*
CL versus D1	.0012	<.0001*	<.0001*	<.0001*	<.0001*	.0014	<.0001*	<.0001*	.0965	.6865	<.0001*	<.0001*	<.0001*	.0039
FT versus D1	.1304	<.0001*	<.0001*	<.0001*	<.0001*	.3581	<.0001*	<.0001*	<.0001*	.6022	<.0001*	.0385	<.0001*	<.0001*
RT versus D1	.2478	.328	<.0001*	<.0001*	<.0001*	.4147	<.0001*	<.0001*	<.0001*	<.001*	<.0001*	<.0001*	<.0001*	<.0001*
TF versus D1	.0015	.9007	<.001*	.0022	<.0001*	<.0001*	.7412	.0067	.003	.0234	<.0001*	<.0001*	<.0001*	<.0001*
AC versus D2	.0023	<.0001*	<.0001*	.1266	.9357	.3354	<.0001*	.0039	<.0001*	<.0001*	<.0001*	<.0001*	<.001*	<.0001*
CC versus D2	.0906	.0747	<.0001*	<.0001*	<.0001*	.0532	.0055	<.0001*	.0142	.0032	<.0001*	.3738	<.0001*	<.001*
CL versus D2	.0058	<.0001*	<.0001*	<.0001*	<.0001*	.1922	<.0001*	<.0001*	<.0001*	<.001*	.5229	<.0001*	<.0001*	<.0001*
FT versus D2	.6228	.0462	<.0001*	<.0001*	<.0001*	.0155	<.0001*	<.0001*	<.0001*	.0446	<.0001*	<.0001*	<.0001*	<.0001*
RT versus D2	.0415	.0043	<.0001*	<.0001*	<.0001*	.0136	<.0001*	<.0001*	<.0001*	<.0001*	<.0001*	<.0001*	<.0001*	<.0001*
TF versus D2	.0027	<.001*	<.0001*	<.0001*	<.0001*	<.0001*	.0105	<.0001*	.1727	.8087	<.0001*	.328	<.0001*	<.0001*
AC versus M1	.0105	<.0001*	<.0001*	.398	.1922	.9474	<.0001*	<.0001*	<.0001*	<.0001*	<.0001*	<.0001*	<.0001*	.2996
CC versus M1	.4492	.1462	.0035	<.0001*	<.0001*	.0013	<.0001*	<.0001*	.0001*	<.0001*	<.0001*	<.0001*	.0035	.2025
CL versus M1	.4946	<.0001*	<.0001*	<.0001*	<.0001*	.0234	<.0001*	<.0001*	<.0001*	<.0001*	<.0001*	<.0001*	.0162	<.0001*
FT versus M1	.0029	<.0001*	<.0001*	<.0001*	<.0001*	.0906	<.0001*	<.0001*	<.0001*	<.0001*	<.0001*	<.0001*	<.0001*	<.0001*
RT versus M1	.0096	.2665	<.0001*	<.0001*	<.0001*	.0462	<.0001*	<.0001*	<.0001*	.01	<.0001*	<.0001*	<.0001*	<.0001*
TF versus M1	.0371	.6228	.0032	<.0001*	<.0001*	<.0001*	<.0001*	<.0001*	.0037	<.0001*	<.0001*	<.0001*	<.0001*	.0591
AC versus M2	.0332	<.0001*	.0001*	<.0001*	<.0001*	<.0001*	<.0001*	.0332	<.0001*	.1342	<.0001*	<.0001*	<.0001*	<.0001*
CC versus M2	.7973	.0878	.9007	.6543	<.0001*	<.0001*	<.0001*	<.0001*	<.0001*	<.0001*	<.0001*	.085	.1823	<.0001*
CL versus M2	.924	<.0001*	<.0001*	.0965	<.0001*	<.0001*	<.0001*	<.0001*	<.0001*	.1591	<.001*	<.0001*	.04	.0115
FT versus M2	.043	.0654	<.0001*	.0371	<.001*	<.0001*	<.0001*	<.0001*	<.0001*	.843	<.0001*	<.0001*	<.0001*	<.0001*
RT versus M2	.0263	.0052	<.0001*	<.0001*	<.0001*	<.0001*	<.0001*	<.0001*	<.0001*	.04	<.0001*	<.0001*	<.0001*	<.0001*
TF versus M2	.1304	<.001*	.6125	.2188	<.0001*	<.0001*	<.0001*	.0058	<.0001*	.0017	<.0001*	.924	<.001*	<.0001*

TABLE 1 (Continued)

	VHF	PSR	COL-I	COL-II	COL-III	COL-IV	AB	SO	PAS	VCAN	ACAN	KS	C6S	TNC
AC versus P1	.1547	<.0001*	<.0001*	<.0001*	.0183	<.001*	<.0001*	<.0001*	<.0001*	<.0001*	<.0001*	<.0001*	<.0001*	<.0001*
CC versus P1	.5039	<.0001*	<.0001*	.1504	<.0001*	.4853	.0063	<.001*	<.0001*	.0274	<.0001*	.1194	<.001*	<.0001*
CL versus P1	.0654	<.0001*	<.0001*	<.001*	<.0001*	.1058	<.0001*	.0878	<.0001*	<.0001*	<.0001*	<.0001*	.0029	<.0001*
FT versus P1	.0002	<.0001*	<.0001*	.3208	<.0001*	<.0001*	<.0001*	.4317	<.0001*	.0191	<.0001*	<.001*	<.0001*	<.001*
RT versus P1	.0019	<.0001*	<.0001*	<.0001*	<.0001*	<.0001*	<.0001*	.0023	<.0001*	<.0001*	<.0001*	<.0001*	<.0001*	<.0001*
TF versus P1	.4232	<.0001*	<.0001*	.008	<.0001*	<.0001*	.1547	<.0001*	<.0001*	.3354	<.0001*	<.001*	<.0001*	<.0001*
AC versus P2	.1504	<.0001*	<.0001*	<.0001*	<.0001*	<.0001*	<.0001*	<.0001*	<.0001*	.0125	<.0001*	<.0001*	<.0001*	<.0001*
CC versus P2	.5229	.2478	<.0001*	<.001*	<.0001*	.0073	<.0001*	<.0001*	<.0001*	<.0001*	.0225	.0015	.0142	<.0001*
CL versus P2	.0191	<.0001*	<.0001*	.2132	<.0001*	.001	<.0001*	<.0001*	<.0001*	.2861	<.0001*	<.0001*	.0115	<.0001*
FT versus P2	.0001	.0052	<.0001*	<.001*	<.0001*	<.0001*	<.0001*	<.0001*	<.0001*	.7412	<.0001*	<.0001*	<.0001*	<.0001*
RT versus P2	.0001	.011	<.0001*	<.0001*	<.0001*	<.0001*	<.0001*	<.0001*	<.0001*	.0162	.0023	<.0001*	<.0001*	<.0001*
TF versus P2	.2665	.0063	<.0001*	.2665	<.0001*	<.0001*	<.0001*	<.0001*	<.0001*	.0009	.0017	.1635	<.0001*	<.0001*
D1 versus D2	.0878	<.0001*	<.0001*	.0115	<.0001*	.0149	<.001*	.0878	<.0001*	.0076	<.0001*	<.0001*	.665	<.0001*
M1 versus M2	.6333	<.0001*	.0063	<.0001*	<.0001*	<.0001*	.0797	<.0001*	<.0001*	<.0001*	<.0001*	<.0001*	.0285	<.0001*
P1 versus P2	.5619	<.0001*	.1727	<.0001*	<.0001*	.4671	<.0001*	<.0001*	<.001*	<.0001*	<.0001*	<.0001*	.1922	.9941

Note: For each histochemical and immunohistochemical method, average intensity units (IU) ± standard deviation values are shown for each sample. Statistical *p* values correspond to the comparison of each SLIL zone versus each control tissue and between both zones of each region using the Mann-Whitney test. Statistically significant *p* values below .001 are labeled with asterisks (*).

Abbreviations: AB, alcian blue histochemistry for proteoglycans; AC, articular cartilage; CC, carpal articular capsule; CL, carpal ligament; COL-I, COL-II, COL-III and COL-IV, immunohistochemistry for collagens types I, II, III and IV, respectively; D1, dorsal region (part 1); D2, dorsal region (part 2); FT, flexor tendon; M1, membranous region (part 1); M2, membranous region (part 2); P1, palmar region (part 1); P2, palmar region (part 2); PAS, periodic acid-Schiff histochemistry for glycosaminoglycans; PSR, picrosirius red histochemistry for collagen fibers; RT, retinaculum; SO, safranin O histochemistry for cartilage components; TF, triangular fibrocartilage; VHF, Verhoeff histochemistry for elastic fibers; VCAN, ACAN, KS, C6S and TNC, immunohistochemistry for versican, aggrecan, keratan-sulphate, chondroitin-6-sulphate and tenascin-C.

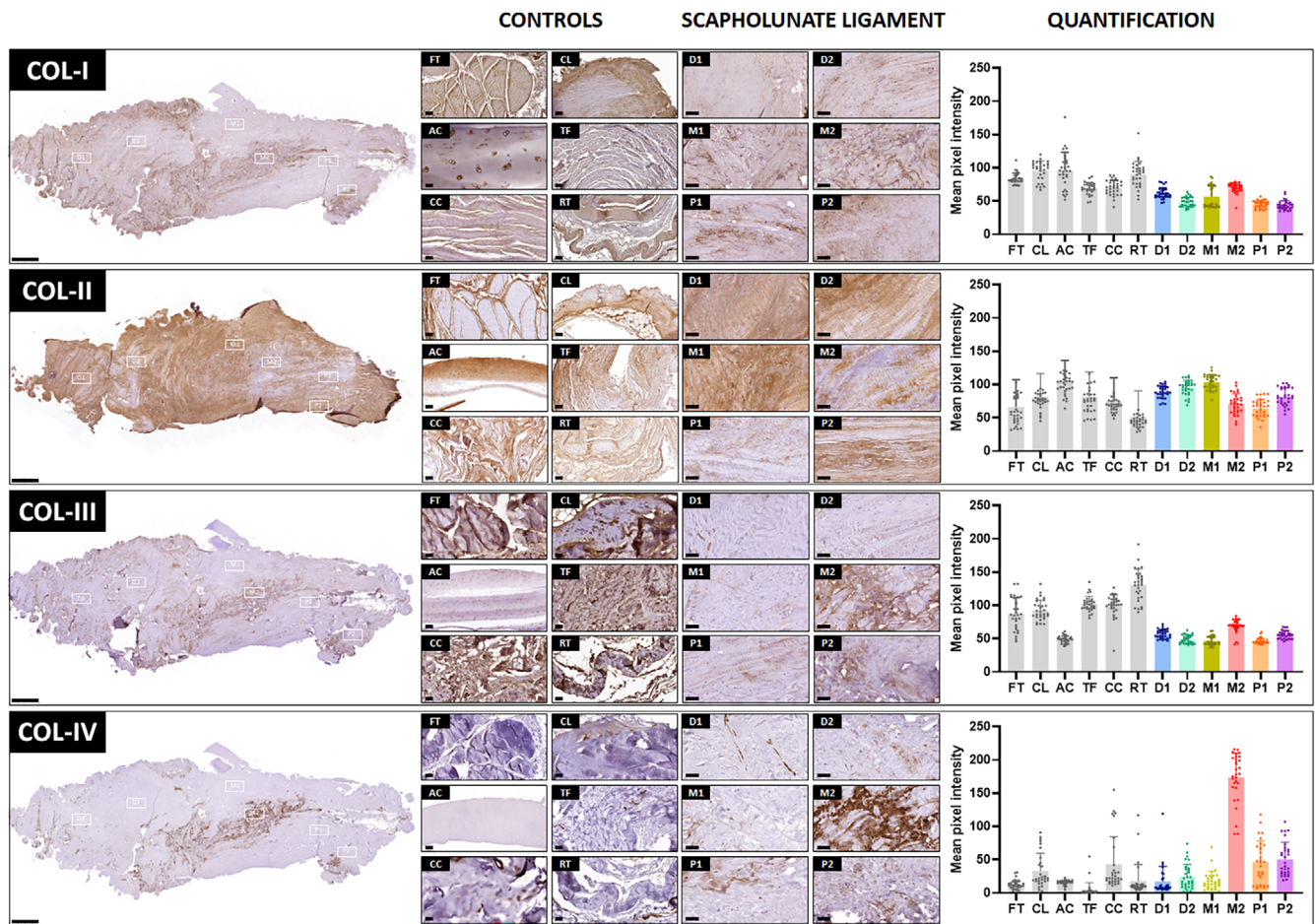


FIGURE 4 Analysis of collagen types I, II, III and IV in the human scapholunate ligament (SLIL) and control tissues as determined by immunohistochemistry. Histograms represent the results of the staining signal quantification for each analysis technique. AC, articular cartilage; CC, carpal articular capsule; CL, carpal ligament; D1, dorsal region (part 1); D2, dorsal region (part 2); FT, flexor tendon; M1, membranous region (part 1); M2, membranous region (part 2); P1, palmar region (part 1); P2, palmar region (part 2); RT, retinaculum; TF, triangular fibrocartilage. Scale bars: 1000 μm in the SLIL global image and 100 μm in the high magnification images.

Then, aggrecan analysis showed high intensity in AC and in M1 and D1 regions, with non-significant differences between D1 and AC (Figure 6 and Table 1). KS and C6S were abundant in all SLIL regions, although keratan-sulphate was preferentially found in M1, with significantly higher staining signal than all control tissues. Finally, tenascin C tended to show very low expression in all the analyzed tissues, with the highest intensity found in the RT control tissue (significantly higher than all SLIL regions), and in M2 and D1 regions (significantly higher than all other control tissues except CL) (Figure 6 and Table 1).

3.3 | Characterization of the human scapholunate ligament cell populations and blood vessels

To determine the phenotype of the cells found at the different regions of the SLIL, we first carried out an immunohistochemical analysis of S100 expression. As shown in Figure 7 and Table 2, our results show that the zones that were more enriched in S100-positive cells was M1, followed by D2 and M2, whereas the zone with lower content of positive cells was D1. Differences between D1 and the rest of SLIL

zones were statistically significant, as well as the differences between P1 and D2 and M1 and between P2 and D2 and M1. Then, we analyzed the expression of the undifferentiation marker CD73, and we found that all regions contained cells showing positive signal for this marker, although the highest number of positive cells corresponded to D2, and the lowest, to P2. Differences between D2 and D1, P1 and P2 were statistically significant (Figure 7 and Table 2).

In order to evaluate the distribution of the blood vessels in the SLIL, we quantified these structures in each zone of the SLIL after labeling the vessels using CD34 immunohistochemistry. As shown in Figure 7 and Table 2, our analysis revealed that blood vessels were abundant in D1, D2, P1 and P2, but were very scarce in M1 and M2. Differences between M1 or M2 and the rest of zones were statistically significant.

3.4 | Hierarchical classification of the human scapholunate ligament

Once we quantified thirteen relevant ECM components showing statistical differences among the different samples (all markers except

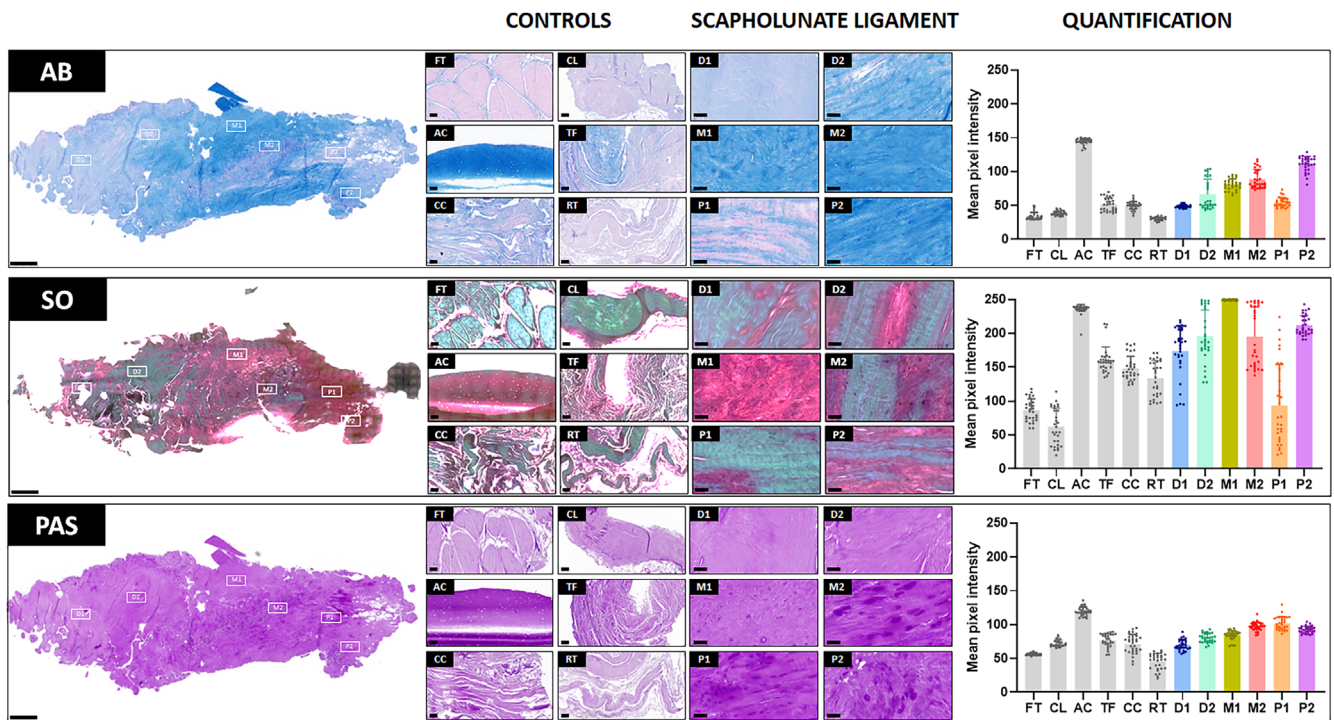


FIGURE 5 Analysis of proteoglycans and glycoproteins in the human scapholunate ligament (SLIL) and control tissues as determined by alcian blue (AB), safranin O (O) and Periodic acid-Schiff (PAS) histochemistry. Histograms represent the results of the staining signal quantification for each analysis technique. AC, articular cartilage; CC, carpal articular capsule; CL, carpal ligament; D1, dorsal region (part 1); D2, dorsal region (part 2); FT, flexor tendon; M1, membranous region (part 1); M2, membranous region (part 2); P1, palmar region (part 1); P2, palmar region (part 2); RT, retinaculum; TF, triangular fibrocartilage. Scale bars: 1000 μ m in the SLIL global image and 100 μ m in the high magnification images.

VHF), we classified the analyzed tissues based on their global profile for these ECM components using hierarchical clustering. As shown in Figure 8, our results showed two main groups of samples. In the first branch, we found five out of the six control tissues analyzed here: FT, RT, CL, TF, and CC. In the second branch, however, we found all our six SLIL zones (M2, P1, D1, M1, D2, and P2) clustering together with AC control tissues. Interestingly, AC clustered together with M1, with both types of tissues forming an independent classification subbranch.

4 | DISCUSSION

Despite its crucial role as a major stabilizer of the wrist bones, the exact structure of the human SLIL is not properly understood. For this reason, in the present study, we evaluated the human SLIL using an array of histological, histochemical and immunohistochemical methods, trying to shed light on the specific composition of each zone of the SLIL. In the first place, we analyzed each SLIL region after establishing two subregions in each of the classically defined regions (dorsal, membranous and palmar) (Berger, 1996; Berger et al., 1991). This subdivision of each region was done to define the histological characteristics of each zone of the ligament with higher precision. In fact, the original classification was made based on the gross aspect of the SLIL, what may not coincide with the histological features of each zone of the SLIL.

The results of our histological analysis revealed that the SLIL was heterogeneous, and each subregion had specific histological characteristics. First, our histological analysis using HE (Figure 2) staining confirmed that the dorsal region of the SLIL consisted of a dense ECM with dispersed elongated cells that partially resembles a human ligament, as other authors already demonstrated (Berger, 1996; Berger et al., 1991; Berger & Blair, 1984; Sokolow & Saffar, 2001). However, the three-dimensional disposition of the fibers and the cell distribution were different in both subregions of this area (D1 and D2), which supports the idea that the dorsal area consisted of two distinct zones. Then, the analysis of the membranous region revealed the presence of a dense tissue containing cells resembling human chondrocytes that were surrounded by a well-defined pericellular matrix and a capsule, as it is the case of the human cartilage. Although the similitude of the membranous region with human fibrocartilage was previously preconized (Berger, 1996; Berger et al., 1991; Berger & Blair, 1984), we found that the ECM was more dense in M2 than in M1, and both the cells and the ECM in M1 were more similar to hyaline chondrocytes than to fibrochondrocytes, supporting again the possibility that both subregions could be histologically different. Finally, our characterization of the palmar region revealed a structure containing abundant fibers and scattered spindle-shaped cells, as previously described (Berger, 1996; Berger et al., 1991; Berger & Blair, 1984). Again, differences in fiber orientation and cell content were detected between P1 and P2, suggesting again that this region could be heterogeneous.

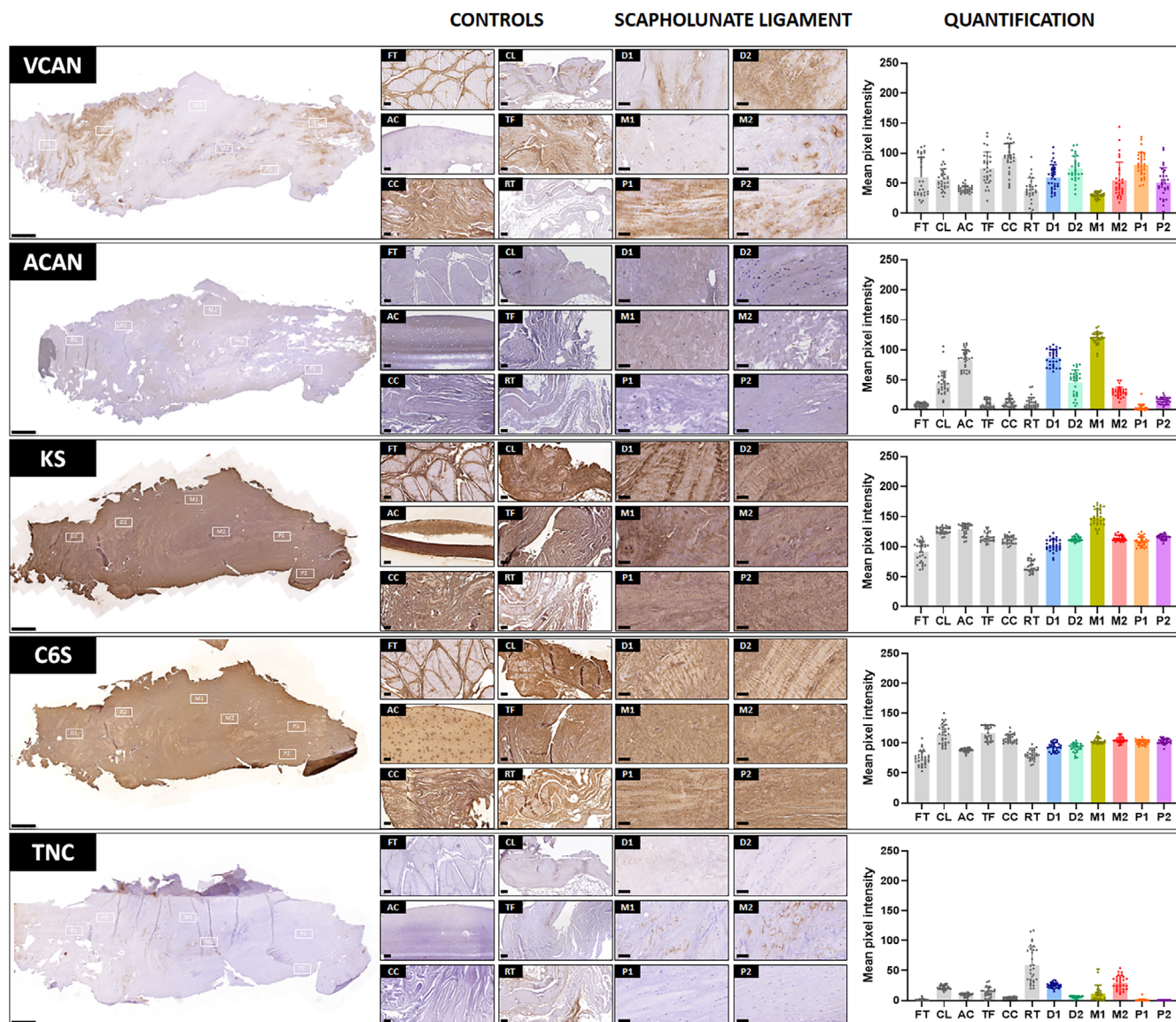


FIGURE 6 Analysis of specific proteoglycans, glycosaminoglycans and glycoproteins molecules in the human scapholunate ligament (SLIL) and control tissues as determined by immunohistochemistry. Versican (VCAN) and aggrecan (ACAN) were identified by indirect immunohistochemistry alongside with keratan-sulphate (KS), chondroitin-6-sulphate (C6S) and tenascin-C (TNC). Histograms represent the results of the staining signal quantification for each analysis technique. AC, articular cartilage; CC, carpal articular capsule; CL, carpal ligament; D1, dorsal region (part 1); D2, dorsal region (part 2); FT, flexor tendon; M1, membranous region (part 1); M2, membranous region (part 2); P1, palmar region (part 1); P2, palmar region (part 2); RT, retinaculum; TF, triangular fibrocartilage. Scale bars: 1000 μm in the SLIL global image and 100 μm in the high magnification images.

To confirm our hypothesis that each region could be heterogeneous, we analyzed the ECM composition at each subregion. The ECM plays a key role in controlling the physical properties of human tissues, supporting compressive and extension forces and providing resilience and shock absorption capacity, especially during continuous biomechanical stress (Hoffmann et al., 2019). For this reason, understanding of the ECM configuration at each subregion of the SLIL could contribute to understand the pathomechanics of the human carpus (Wolff & Wolfe, 2016). In this milieu, we first analyzed the presence of ECM fibers in the SLIL and compared the results with control tissues (Figure 3). Regarding elastic fibers, we found that these

components were very scarcely present in the SLIL and in control tissues. Although elastic fibers have been found in high amounts at certain ligaments such as the nuchal ligament or the ligamentum flavum, its presence is location-specific, and many ligaments have very low amounts of these fibers (Hill et al., 2020). Despite the low amount of elastic fiber found within the SLIL, it is probably that these fibers, which run parallelly to the collagen networks, contribute to the resistance of this complex structure to tensile or shear stress (Henninger et al., 2019).

Then, we analyzed the presence and distribution of collagen fibers. Collagen is the main fibrillar component of the ECM and plays

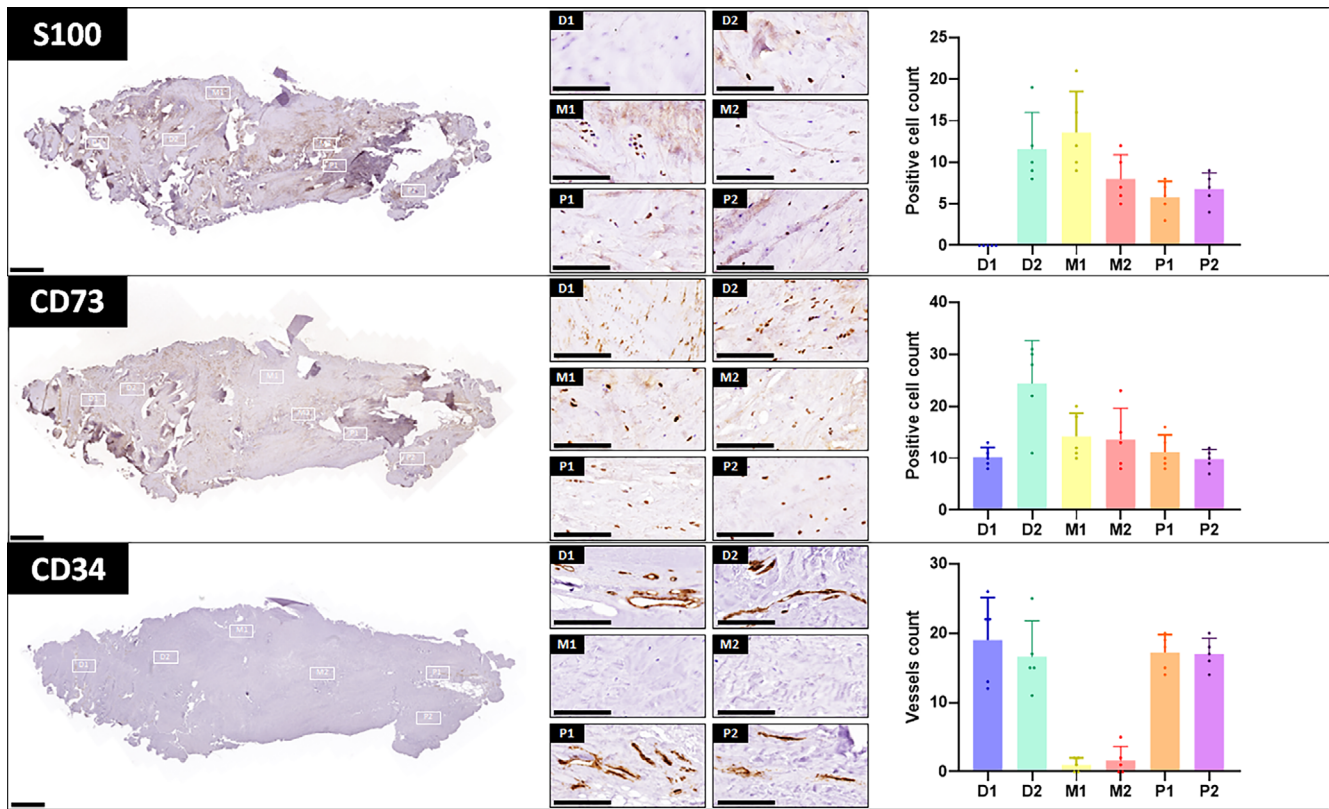


FIGURE 7 Analysis of expression of the cell markers S100 and CD73 and quantification of CD34-positive blood vessels in the different regions of the human scapholunate ligament (SLIL). Histograms represent the results of the quantitative analysis as number of positive cells or number of blood vessels per unit of area. AC, articular cartilage; CC, carpal articular capsule; CL, carpal ligament; D1, dorsal region (part 1); D2, dorsal region (part 2); FT, flexor tendon; M1, membranous region (part 1); M2, membranous region (part 2); P1, palmar region (part 1); P2, palmar region (part 2); RT, retinaculum; TF, triangular fibrocartilage. Scale bars: 1000 μ m in the SLIL global image and 100 μ m in the high magnification images.

a crucial role in controlling tissue stiffness and resistance to tensile forces, as these fibers can store elastic energy by stretching the flexible regions of the fibrils in their triple-helix tridimensional structure (Silver et al., 2003, 2021). Collagen fibers are typically very abundant in mature tendons and ligaments (Barros et al., 2002) and in other mechanically demanding areas, where they are the main responsible for mechanotransduction of incoming forces. As expected, we found that all SLIL regions and control tissues contained high amounts of collagen fibers (Figures 3 and 4), with some differences among samples. Among controls, the higher concentration of collagen was found in AC, which is known to contain high amounts of these fibers (Bloebaum et al., 2021). Regarding the SLIL, the highest contents of collagen fibers were found in D1 and M1, whereas the lowest amounts of collagen corresponded to both subregions of the palmar region (P1 and P2). These results are in agreement with previous biomechanical studies suggesting that the palmar region could be mechanically weaker than the dorsal region (Kakar et al., 2019), and could contribute to understand why most SLIL lesions begin with a disruption of the palmar region of this structure (Andersson & Garcia-Elias, 2013). Interestingly, differences between both subregions of each region (D1 vs. D2, M1 vs. M2 and P1 vs. P2) were statistically significant, suggesting again that each region could be heterogeneous.

Strikingly, our analysis of specific types of collagens (Figure 4) also revealed some differences among areas. Collagen type II was abundant in all SLIL regions, with the highest staining intensity corresponding to M1 and AC, and the strongest immunohistochemical signal for collagens types I, III and IV was found in M2. These results are in agreement with previous studies that also identified Col-I, Col-II and Col-III in different SLIL regions, although no subregions were analyzed in these studies (Milz et al., 2006). Our findings showing high heterogeneity among the subregions of the SLIL supports the idea that the classical SLIL regions are diverse and should be subdivided in smaller parts showing unique biological and histological properties. Although some SLIL regions showed similarities with the human ligament, other regions were more similar to the articular cartilage, especially, M1.

In addition, we assessed the presence of relevant non-fibrillar components of the ECM in the tissues analyzed in this work (Figures 5 and 6). Non-fibrillar ECM components are fundamental molecules able to control the biomechanical properties of human tissues by regulating the tissue response to external mechanical forces (Ghadie et al., 2021). Specifically, proteoglycans and glycosaminoglycans mediate collagen fibrils alignment and regulate water content of the ECM, which in turn, is able to control tissue stiffness (Müller et al., 2004; Smith & Melrose, 2015). Our results showed that the

TABLE 2 Quantitative analysis of cell phenotype and blood vessel quantification in the human scapholunate ligament (SLIL) zones.

	S100	CD73	VESSELS
D1	0.4 ± 0.55	10.2 ± 1.92	19 ± 6.16
D2	11.6 ± 4.39	24.4 ± 8.26	16.6 ± 5.18
M1	13.6 ± 4.93	14.2 ± 4.49	1 ± 1
M2	8 ± 2.92	13.6 ± 5.98	1.6 ± 2.07
P1	5.8 ± 1.92	11.2 ± 3.27	17.2 ± 2.59
P2	6.8 ± 1.92	9.8 ± 1.92	17 ± 2.24
D1 versus D2	<.0001*	.0003*	.4813
D1 versus M1	<.0001*	.0232	<.0001*
D1 versus M2	<.0001*	.2475	<.0001*
D1 versus P1	<.0001*	.6842	.4813
D1 versus P2	<.0001*	.7959	.4813
D2 versus M1	.2475	.0052	<.0001*
D2 versus M2	.0524	.0089	<.0001*
D2 versus P1	<.0001*	.0007*	.4813
D2 versus P2	.0007*	.0003*	.3930
M1 versus M2	.0089	.6842	.7959
M1 versus P1	<.0001*	.0753	<.0001*
M1 versus P2	<.0001*	.0147	<.0001*
M2 versus P1	.1431	.5787	<.0001*
M2 versus P2	.4813	.1431	<.0001*
P1 versus P2	.2475	.4813	.7959

Note: For each analysis method, the average number of positive cells or the average number of blood vessels per unit of area ± standard deviation is shown for each sample. Statistical *p* values correspond to the comparison of each SLIL region versus the rest of the regions using the Mann–Whitney test. Statistically significant *p* values below .001 are labeled with asterisks (*).

Abbreviations: AC, articular cartilage; CC, carpal articular capsule; CD73, immunohistochemistry for the stem cell marker CD73; CL, carpal ligament; FT, flexor tendon; D1, dorsal region (part 1); D2, dorsal region (part 2); M1, membranous region (part 1); M2, membranous region (part 2); P1, palmar region (part 1); P2, palmar region (part 2); RT, Retinaculum; S100, immunohistochemistry for the chondrocyte marker S100; TF, triangular fibrocartilage; Vessels, quantification of blood vessels showing positive immunohistochemical signal for CD34.

human SLIL was enriched in these components, and proteoglycans and glycoproteins tended to be more abundant in SLIL than in control tissues, with the exception of AC, which showed the highest contents of all control tissues. Remarkably, safranin O staining, which is able to identify relevant components of the human cartilage, mainly, proteoglycans, showed high intensity in AC, as expected, but also in M1, and none of these tissues showed positive staining for collagen bundles, as determined by this technique. These results point out the possibility that M1 could resemble the histological composition of the human articular cartilage. When versican was analyzed, we found that the lowest expression of this proteoglycan corresponded to AC and M1 (Figure 6). Again, significant differences were found between both subregions of the dorsal, membranous and palmar regions for all non-fibrillar components, except for some specific comparisons. Analysis

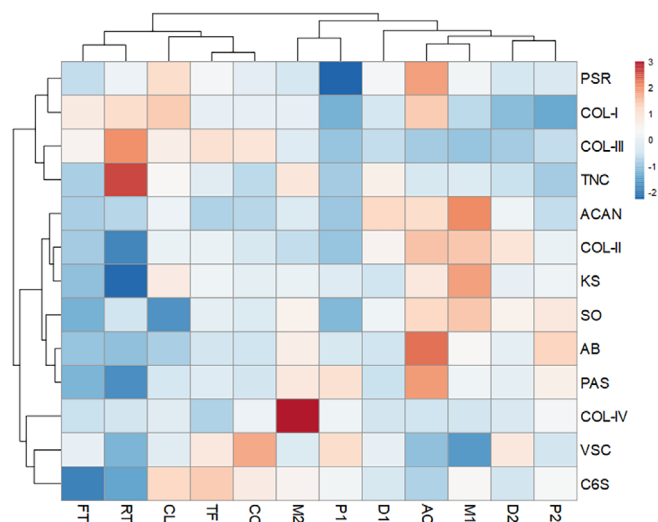


FIGURE 8 Hierarchical clustering analysis of the tissues analyzed in this work (controls and human scapholunate ligament -SLIL- zones) based on the quantitative analysis of ECM composition. AC, articular cartilage; CC, carpal articular capsule; CL, carpal ligament; D1, dorsal region (part 1); D2, dorsal region (part 2); FT, flexor tendon; M1, membranous region (part 1); M2, membranous region (part 2); P1, palmar region (part 1); P2, palmar region (part 2); RT, retinaculum; TF, triangular fibrocartilage. Tissues with high relative signal for each analysis method are represented in red, whereas tissues with the lowest signal appear in blue.

of aggrecan revealed a high immunostaining intensity in the M1 sub-region, along with the AC. Aggrecan, a proteoglycan primarily composed of chondroitin sulfate and keratan sulfate, plays a crucial role in maintaining tissue hydration and providing compressive strength, particularly in cartilage (Kiani et al., 2002). Similarly, the two major glycosaminoglycans normally found in human cartilage (KS and C6S) were found at high levels in most analyzed tissues, with the highest expression of KS corresponding to M1 and AC. These results are in agreement with our hypothesis that M1 could structurally resemble the histological composition of the human articular cartilage, in which aggrecan, KS and C6S are very abundant, whereas versican is present at lower levels (Grover & Roughley, 1993). In general, the presence of all these molecules in AC and in M1 could contribute to provide both tissues with specific mechanical properties and water retention. Finally, tenascin C, a glycoprotein involved in modulating cell-matrix interactions, tissue development that is expressed de novo during wound healing and in pathological conditions (Midwood et al., 2016), was found at very low levels in all tissues, suggesting that all the analyzed structures were normal and devoid of any structural alterations.

In order to furtherly characterize each zone of the SLIL, we analyzed the phenotype of cells found at each area using S100 immunohistochemistry (Figure 7), a typical cartilage-linked marker that is especially expressed by hyaline chondrocytes (Yammani, 2012). The finding that cells were positive at the M1 area, followed by M2, along with the ECM structure showing the typical capsule and ECM arrangement of the human cartilage, confirms the cartilaginous nature of these zones. Furthermore, the analysis of blood vessels showed

very few vessels at M1 and M2, as it is the case of cartilage. In general, these results, support the idea that the membranous region could indeed be composed by a variety of cartilage tissue, and that M1 could be more similar to hyaline cartilage than M2.

Finally, we aimed to assess the presence of stem cells at each zone of the SLIL in order to identify those areas that could have higher self-regeneration potential. Our results suggest that, in general, the SLIL contains low amounts of stem cells, what is in agreement with previous reports questioning the intrinsic healing capability of the human SLIL (Figure 7) (Minami et al., 2003). However, the fact that subregion D2 could be more enriched in stem cells than other areas may imply that the dorsal area has more intrinsic regenerative potential, what could be related to the presence of stronger mechanical forces affecting the dorsal region of the SLIL, as compared with other regions (Kakar et al., 2019).

Altogether, these results support our hypothesis that each region of the human SLIL could be structurally heterogeneous. In fact, a global analysis of the ECM evaluation results using hierarchical clustering confirmed the existence of differences within the SLIL (Figure 8). Remarkably, all subdivisions of SLIL clustered together in the same branch, along with the AC control tissue. These results suggest that all SLIL zones shared ECM similarities with hyaline cartilage (AC), with M1 showing the closest distance with AC. Although the SLIL is generally considered to be histologically related to a human fibrocartilage (Berger, 1996; Sokolow & Saffar, 2001), our comprehensive analysis suggests that this structure could be more close to an articular cartilage, with high heterogeneity among zones.

The present study has several limitations. First, results should be confirmed in a larger cohort of human hand donors. Second, biomechanical studies should be carried out in the future to correlate our histological results with biomechanical data of stiffness and elasticity of each specific zone of the SLIL. Finally, the study could be complemented with the implant of different biomaterials or bioartificial tissues generated by tissue engineering to determine the potential usefulness of this approach to repair the human SLIL, as previously reported for other wrist ligaments (Lui et al., 2021).

To our knowledge, this is the first study that characterized the SLIL after establishing a subclassification of the classical SLIL regions. Overall, our results support the idea that each subregion has a definite structure and composition not only at a morphological level, but also when the expression of relevant tissue components were analyzed. These results could be clinically relevant, as they could contribute to explain why most disruptions of the human SLIL typically commence at the palmar region, and support the surgical approaches based on a reinforcement of this region. In addition, the higher similitude of the SLIL with a cartilage-like tissue contributes to understand the poor regenerative properties of the human SLIL, especially in the areas devoid of blood vessels. However, the heterogeneity of this structure supports the idea that certain zones, such as D2, could have more intrinsic regeneration potential derived from the presence of stem cells. In consequence, lesions affecting the zones with lower regeneration potential, especially M1 and M2, should be treated with the use of tissue grafts containing

mesenchymal stem cells or other approaches based on tissue engineering and regenerative medicine, as suggested for the human knee meniscus (Kwon et al., 2019). In addition, our results suggest that surgical repair of injuries affecting the membranous region should preferentially be repaired using cartilage grafts that can be obtained from articular surfaces, meniscus grafts or other similar anatomical regions, as described for the knee joint repair (Ashton Tan et al., 2022). However, surgical treatment of the dorsal region of the SLIL could be favored by the use of grafts whose histological structure is more similar to this region, such as the human ligaments and tendons. Future works carried out in vivo should confirm or not this statement.

AUTHOR CONTRIBUTIONS

Jesús Chato-Astrain: Conceptualization; investigation; methodology; data curation; writing – original draft. **Olga Roda:** Conceptualization; investigation; methodology. **Víctor Carriel:** Conceptualization; investigation; methodology; data curation. **Fidel Hita-Contreras:** Conceptualization; investigation; methodology. **Indalecio Sánchez-Montesinos:** Conceptualization; methodology; data curation; investigation. **Miguel Alaminos:** Methodology; data curation; conceptualization; investigation; writing – review and editing; formal analysis. **Pedro Hernández-Cortés:** Conceptualization; investigation; methodology; data curation; writing – review and editing.

ACKNOWLEDGMENTS

Supported by CTS-115, Tissue Engineering Group of the University of Granada, Spain. Funding for open access charge: Universidad de Granada / CBUA.

CONFLICT OF INTEREST STATEMENT

Authors declare that they do not have any conflicts of interest.

DATA AVAILABILITY STATEMENT

The data that support the findings of this study are openly available at <https://doi.org/10.5281/zenodo.8356862>.

ORCID

Jesús Chato-Astrain  <https://orcid.org/0000-0002-2378-2696>

Olga Roda  <https://orcid.org/0000-0001-8696-6313>

Víctor Carriel  <https://orcid.org/0000-0002-8114-5644>

Fidel Hita-Contreras  <https://orcid.org/0000-0001-7215-5456>

Indalecio Sánchez-Montesinos  <https://orcid.org/0000-0001-9141-7079>

Miguel Alaminos  <https://orcid.org/0000-0003-4876-2672>

Pedro Hernández-Cortés  <https://orcid.org/0000-0003-2057-5285>

REFERENCES

- Andersson, J. K. (2017). Treatment of scapholunate ligament injury: Current concepts. *EFORT Open Reviews*, 2(9), 382–393. <https://doi.org/10.1302/2058-5241.2.170016>
- Andersson, J. K., & García-Elias, M. (2013). Dorsal scapholunate ligament injury: A classification of clinical forms. *The Journal of Hand Surgery, European*, 38(2), 165–169. <https://doi.org/10.1177/1753193412441124>

- Ashton Tan, K. S., Kiat Chua, S. K., Heng Yeo, E. Y., & Bin Abd Razak, H. R. (2022). Two to 14 year outcomes of combined meniscal allograft transplantation with anterior cruciate ligament reconstruction: A systematic review. *Arthroscopy: The Journal of Arthroscopic & Related Surgery: Official Publication of the Arthroscopy Association of North America and the International Arthroscopy Association*, 50749-8063(22), 00700-9. <https://doi.org/10.1016/j.arthro.2022.10.042>
- Barros, E. M. K. P., Rodrigues, C. J., Rodrigues, N. R., Oliveira, R. P., Barros, T. E. P., & Rodrigues, A. J. (2002). Aging of the elastic and collagen fibers in the human cervical interspinous ligaments. *The Spine Journal: Official Journal of the North American Spine Society*, 2(1), 57-62. [https://doi.org/10.1016/s1529-9430\(01\)00167-x](https://doi.org/10.1016/s1529-9430(01)00167-x)
- Berger, R. A. (1996). The gross and histologic anatomy of the scapholunate interosseous ligament. *The Journal of Hand Surgery*, 21(2), 170-178. [https://doi.org/10.1016/S0363-5023\(96\)80096-7](https://doi.org/10.1016/S0363-5023(96)80096-7)
- Berger, R. A., & Blair, W. F. (1984). The radioscapulohumeral ligament: A gross and histologic description. *The Anatomical Record*, 210(2), 393-405. <https://doi.org/10.1002/ar.1092100215>
- Berger, R. A., Kauer, J. M., & Landsmeer, J. M. (1991). Radioscapulohumeral ligament: A gross anatomic and histologic study of fetal and adult wrists. *The Journal of Hand Surgery*, 16(2), 350-355. [https://doi.org/10.1016/s0363-5023\(10\)80125-x](https://doi.org/10.1016/s0363-5023(10)80125-x)
- Blanco-Elices, C., Chato-Astrain, J., González-González, A., Sánchez-Porras, D., Carriel, V., Fernández-Valadés, R., Sánchez-Quevedo, M. D. C., Alaminos, M., & Garzón, I. (2022). Histological profiling of the human umbilical cord: A potential alternative cell source in tissue engineering. *Journal of Personalized Medicine*, 12(4), 648. <https://doi.org/10.3390/jpm12040648>
- Bloebaum, R. D., Wilson, A. S., & Martin, W. N. (2021). A review of the collagen orientation in the articular cartilage. *Cartilage*, 13(2_suppl), 367S-374S. <https://doi.org/10.1177/1947603520988770>
- Carriel, V., Garzon, I., Campos, A., Cornelissen, M., & Alaminos, M. (2014). Differential expression of GAP-43 and neurofilament during peripheral nerve regeneration through bio-artificial conduits. *Journal of Tissue Engineering and Regenerative Medicine*, 11, 553-563. <https://doi.org/10.1002/term.1949>
- Carriel, V. S., Aneiros-Fernandez, J., Arias-Santiago, S., Garzón, I. J., Alaminos, M., & Campos, A. (2011). A novel histochemical method for a simultaneous staining of melanin and collagen fibers. *The Journal of Histochemistry and Cytochemistry: Official Journal of the Histochemistry Society*, 59(3), 270-277. <https://doi.org/10.1369/0022155410398001>
- García-García, Ó. D., El Soury, M., González-Quevedo, D., Sánchez-Porras, D., Chato-Astrain, J., Campos, F., & Carriel, V. (2021). Histological, biomechanical, and biological properties of Genipin-crosslinked decellularized peripheral nerves. *International Journal of Molecular Sciences*, 22(2), E674. <https://doi.org/10.3390/ijms22020674>
- García-Martínez, L., Campos, F., Godoy-Guzmán, C., Del Carmen Sánchez-Quevedo, M., Garzón, I., Alaminos, M., Campos, A., & Carriel, V. (2017). Encapsulation of human elastic cartilage-derived chondrocytes in nanostructured fibrin-agarose hydrogels. *Histochemistry and Cell Biology*, 147(1), 83-95. <https://doi.org/10.1007/s00418-016-1485-9>
- Ghadie, N. M., St-Pierre, J.-P., & Labrosse, M. R. (2021). The contribution of glycosaminoglycans/proteoglycans to aortic mechanics in health and disease: A critical review. *IEEE Transactions on Bio-Medical Engineering*, 68(12), 3491-3500. <https://doi.org/10.1109/TBME.2021.3074053>
- Grover, J., & Roughley, P. J. (1993). Versican gene expression in human articular cartilage and comparison of mRNA splicing variation with aggrecan. *The Biochemical Journal*, 291(Pt 2), 361-367. <https://doi.org/10.1042/bj2910361>
- Henninger, H. B., Ellis, B. J., Scott, S. A., & Weiss, J. A. (2019). Contributions of elastic fibers, collagen, and extracellular matrix to the multi-axial mechanics of ligament. *Journal of the Mechanical Behavior of Biomedical Materials*, 99, 118-126. <https://doi.org/10.1016/j.jmbmm.2019.07.018>
- Hill, J. R., Eekhoff, J. D., Brophy, R. H., & Lake, S. P. (2020). Elastic fibers in Orthopaedics: Form and function in tendons and ligaments, clinical implications, and future directions. *Journal of Orthopaedic Research: Official Publication of the Orthopaedic Research Society*, 38(11), 2305-2317. <https://doi.org/10.1002/jor.24695>
- Hoffmann, G. A., Wong, J. Y., & Smith, M. L. (2019). On force and form: Mechano-biochemical regulation of extracellular matrix. *Biochemistry*, 58(47), 4710-4720. <https://doi.org/10.1021/acs.biochem.9b00219>
- Johnson, J. E., Lee, P., McIlff, T. E., Toby, E. B., & Fischer, K. J. (2013). Scapholunate ligament injury adversely alters in vivo wrist joint mechanics: An MRI-based modeling study. *Journal of Orthopaedic Research: Official Publication of the Orthopaedic Research Society*, 31(9), 1455-1460. <https://doi.org/10.1002/jor.22365>
- Kakar, S., Greene, R. M., Denbeigh, J., & Van Wijnen, A. (2019). Scapholunate ligament internal brace 360 tenodesis (SLITT) procedure: A biomechanical study. *Journal of Wrist Surgery*, 8(3), 250-254. <https://doi.org/10.1055/s-0038-1670682>
- Kiani, C., Chen, L., Wu, Y. J., Yee, A. J., & Yang, B. B. (2002). Structure and function of aggrecan. *Cell Research*, 12(1), 19-32. <https://doi.org/10.1038/sj.cr.7290106>
- Kitay, A., & Wolfe, S. W. (2012). Scapholunate instability: Current concepts in diagnosis and management. *The Journal of Hand Surgery*, 37(10), 2175-2196. <https://doi.org/10.1016/j.jhssa.2012.07.035>
- Kwon, H., Brown, W. E., Lee, C. A., Wang, D., Paschos, N., Hu, J. C., & Athanasiou, K. A. (2019). Surgical and tissue engineering strategies for articular cartilage and meniscus repair. *Nature Reviews Rheumatology*, 15(9), 550-570. <https://doi.org/10.1038/s41584-019-0255-1>
- Lui, H., Bindra, R., Baldwin, J., Ivanovski, S., & Vaquette, C. (2019). Additively manufactured multiphase bone-ligament-bone scaffold for scapholunate interosseous ligament reconstruction. *Advanced Healthcare Materials*, 8(14), e1900133. <https://doi.org/10.1002/adhm.201900133>
- Lui, H., Vaquette, C., Denbeigh, J. M., Bindra, R., Kakar, S., & van Wijnen, A. J. (2021). Multiphase scaffold for scapholunate interosseous ligament reconstruction: A study in the rabbit knee. *Journal of Orthopaedic Research: Official Publication of the Orthopaedic Research Society*, 39(8), 1811-1824. <https://doi.org/10.1002/jor.24785>
- McHanwell, S., Brenner, E., Chirculescu, A. R. M., Drukker, J., van Mameren, H., Mazzotti, G., Pais, D., Paulsen, F., Plaisant, O., Caillaud, M. M., Laforet, E., Riedere, B. M., Sanudo, J. R., Bueno-Lopez, J. L., Donate-Oliver, F., Sprumont, P., Teofilovski-Parapid, G., & Moxham, B. J. (2008). The legal and ethical framework governing Body Donation in Europe - A review of current practice and recommendations for good practice. *European Journal of Anatomy*, 12(1), 1-24.
- Metsalu, T., & Vilo, J. (2015). ClustVis: A web tool for visualizing clustering of multivariate data using principal component analysis and heatmap. *Nucleic Acids Research*, 43(W1), W566-W570. <https://doi.org/10.1093/nar/gkv468>
- Midwood, K. S., Chiquet, M., Tucker, R. P., & Orend, G. (2016). Tenascin-C at a glance. *Journal of Cell Science*, 129(23), 4321-4327. <https://doi.org/10.1242/jcs.190546>
- Milz, S., Aktas, T., Putz, R., & Benjamin, M. (2006). Expression of extracellular matrix molecules typical of articular cartilage in the human scapholunate interosseous ligament. *Journal of Anatomy*, 208(6), 671-679. <https://doi.org/10.1111/j.1469-7580.2006.00552.x>
- Minami, A., Kato, H., & Iwasaki, N. (2003). Treatment of scapholunate dissociation: Ligamentous repair associated with modified dorsal capsulodesis. *Hand Surgery: An International Journal Devoted to Hand and Upper Limb Surgery and Related Research: Journal of the Asia-Pacific Federation of Societies for Surgery of the Hand*, 8(1), 1-6. <https://doi.org/10.1142/s0218810403001443>
- Müller, L. J., Pels, E., Schurmans, L. R. H. M., & Vrensen, G. F. J. M. (2004). A new three-dimensional model of the organization of proteoglycans and collagen fibrils in the human corneal stroma. *Experimental Eye Research*, 78(3), 493-501. [https://doi.org/10.1016/s0014-4835\(03\)00206-9](https://doi.org/10.1016/s0014-4835(03)00206-9)

- Mullikin, I., Srinivasan, R. C., & Bagg, M. (2020). Current Techniques in Scapholunate Ligament Reconstruction. *The Orthopedic Clinics of North America*, 51(1), 77–86. <https://doi.org/10.1016/j.ocl.2019.09.002>
- Naqui, Z., Khor, W. S., Mishra, A., Lees, V., & Muir, L. (2018). The management of chronic non-arthritis scapholunate dissociation: A systematic review. *The Journal of Hand Surgery, European*, 43(4), 394–401. <https://doi.org/10.1177/1753193417734990>
- Ortiz-Arrabal, O., Carmona, R., García-García, Ó.-D., Chato-Astrain, J., Sánchez-Porras, D., Domezain, A., Oruezabal, R.-I., Carriel, V., Campos, A., & Alaminos, M. (2021). Generation and evaluation of novel biomaterials based on decellularized sturgeon cartilage for use in tissue engineering. *Biomedicine*, 9(7), 775. <https://doi.org/10.3390/biomedicines9070775>
- Rajan, P. V., & Day, C. S. (2015). Scapholunate interosseous ligament anatomy and biomechanics. *The Journal of Hand Surgery*, 40(8), 1692–1702. <https://doi.org/10.1016/j.jhsa.2015.03.032>
- Riederer, B. M., Bolt, S., Brenner, E., Bueno-López, J. L., Circulescu, A. R. M., Davies, D. C., De Caro, R., Gerrits, P. O., McHanwell, S., Pais, D., Paulsen, F., Plaisant, O., Sendemir, E., Stabile, I., & Moxham, B. J. (2012). The legal and ethical framework governing Body Donation in Europe: 1st update on current practice. *European Journal of Anatomy*, 16(1), 1–21.
- Rodríguez-Pozo, J. A., Ramos-Lopez, J. F., Gonzalez-Gallardo, M. C., Campos, F., Sanchez-Porras, D., Oyonarte, S., Oruezabal, R. I., Campos, A., Martín-Piedra, M. A., & Alaminos, M. (2020). Evaluation of myopic cornea lenticules. A histochemical and clinical correlation. *Experimental Eye Research*, 196, 108066. <https://doi.org/10.1016/j.exer.2020.108066>
- Ruiz-López, J., Cardona, J. C., Garzón, I., Pérez, M. M., Alaminos, M., Chato-Astrain, J., & Ionescu, A. M. (2022). Optical behavior of human skin substitutes: Absorbance in the 200–400 nm UV range. *Biomedicine*, 10(7), 1640. <https://doi.org/10.3390/biomedicines10071640>
- Sánchez-Porras, D., Varas, J., Godoy-Guzmán, C., Bermejo-Casares, F., San Martín, S., & Carriel, V. (2023). Histochemical and immunohistochemical methods for the identification of proteoglycans. *Methods in Molecular Biology (Clifton, N.J.)*, 2566, 85–98. https://doi.org/10.1007/978-1-0716-2675-7_7
- Silver, F. H., Freeman, J. W., & Sehra, G. P. (2003). Collagen self-assembly and the development of tendon mechanical properties. *Journal of Biomechanics*, 36(10), 1529–1553. [https://doi.org/10.1016/s0021-9290\(03\)00135-0](https://doi.org/10.1016/s0021-9290(03)00135-0)
- Silver, F. H., Kelkar, N., & Deshmukh, T. (2021). Molecular basis for mechanical properties of ECMs: Proposed role of fibrillar collagen and proteoglycans in tissue biomechanics. *Biomolecules*, 11(7), 1018. <https://doi.org/10.3390/biom11071018>
- Smith, M. M., & Melrose, J. (2015). Proteoglycans in Normal and healing skin. *Advances in Wound Care*, 4(3), 152–173. <https://doi.org/10.1089/wound.2013.0464>
- Sokolow, C., & Saffar, P. (2001). Anatomy and histology of the scapholunate ligament. *Hand Clinics*, 17(1), 77–81.
- Vela-Romera, A., Carriel, V., Martín-Piedra, M. A., Aneiros-Fernández, J., Campos, F., Chato-Astrain, J., Prados-Olleta, N., Campos, A., Alaminos, M., & Garzón, I. (2019). Characterization of the human ridged and non-ridged skin: A comprehensive histological, histochemical and immunohistochemical analysis. *Histochemistry and Cell Biology*, 151(1), 57–73. <https://doi.org/10.1007/s00418-018-1701-x>
- Wolff, A. L., & Wolfe, S. W. (2016). Rehabilitation for scapholunate injury: Application of scientific and clinical evidence to practice. *Journal of Hand Therapy: Official Journal of the American Society of Hand Therapists*, 29(2), 146–153. <https://doi.org/10.1016/j.jht.2016.03.010>
- Yammani, R. R. (2012). S100 proteins in cartilage: Role in arthritis. *Biochimica et Biophysica Acta*, 1822(4), 600–606. <https://doi.org/10.1016/j.bbadis.2012.01.006>

SUPPORTING INFORMATION

Additional supporting information can be found online in the Supporting Information section at the end of this article.

How to cite this article: Chato-Astrain, J., Roda, O., Carriel, V., Hita-Contreras, F., Sánchez-Montesinos, I., Alaminos, M., & Hernández-Cortés, P. (2024). Histological characterization of the human scapholunate ligament. *Microscopy Research and Technique*, 87(2), 257–271. <https://doi.org/10.1002/jemt.24428>